[Research Paper] 대한금속 · 재료학회지 (*Korean J. Met. Mater.*), Vol. 60, No. 8 (2022) pp.593-600
DOI: 10.3365/KJMM.2022.60.8.593

Thermoelectric Performance of Sn and Bi Double-Doped Permingeatite

Hee-Jae Ahn and Il-Ho Kim*

Department of Materials Science and Engineering, Korea National University of Transportation, Chungju 27469, Republic of Korea

Abstract: In this study, mechanical alloying was performed to synthesize permingeatite $Cu_3Sb_{1-x-y}Sn_xBi_ySe_4$ ($0.02 \le x \le 0.06$ and $0.02 \le y \le 0.04$) doped with Sn and Bi. Hot pressing was subsequently conducted to achieve dense sintered bodies. When the Bi content was constant, the carrier concentration increased with the Sn content, but the mobility decreased owing to the increased carrier concentration. In contrast, when the Sn content was constant, the carrier concentration and mobility were not significantly affected by the Bi content. Higher electrical conductivity was observed in specimens with a higher Sn content or lower Bi content; consequently, $Cu_3Sb_{0.92}Sn_{0.06}Bi_{0.02}Se_4$ exhibited the highest electrical conductivity. The Seebeck coefficient increased with temperature, and it is inferred that the permingeatite doped with Sn/Bi does not undergo an intrinsic transition until 623 K. In contrast to the electrical conductivity, a higher Seebeck coefficient was obtained in the specimens with a lower Sn content or higher Bi content; consequently, $Cu_3Sb_{0.94}Sn_{0.02}Bi_{0.04}Se_4$ exhibited the highest Seebeck coefficient. $Cu_3Sb_{0.92}Sn_{0.06}Bi_{0.02}Se_4$ exhibited the maximum power factor, depending on the electrical conductivity and Seebeck coefficient. The electronic thermal conductivity was not significantly affected by temperature, but the lattice thermal conductivity decreased as the temperature increased. However, the thermal conductivity decreased with increasing temperature. Sn doping effectively reduced the lattice thermal conductivity, whereas Bi doping effectively reduced the electronic thermal conductivity; consequently, $Cu_3Sb_{0.94}Sn_{0.02}Bi_{0.04}Se_4$ exhibited the lowest thermal conductivity. Finally, the highest dimensionless figure-of-merit of 0.75 was achieved at 623 K by $Cu_3Sb_{0.92}Sn_{0.06}Bi_{0.02}Se_4$.

(Received 6 April, 2022; Accepted 19 May, 2022)

Keywords: thermoelectric; permingeatite; mechanical alloying; hot pressing; double doping

1. INTRODUCTION

Thermoelectric power generation has attracted significant interest as an eco-friendly and energy-efficient technique because it directly converts waste heat energy into electrical energy [1]. Recently, permingeatite (Cu_3SbSe_4) has been investigated for thermoelectric applications [2]. Cu_3SbSe_4 exhibits a tetragonal (space group $I\bar{4}2$ m) structure, where Cu is ionized into Cu^+ and Cu^{2+} to form distorted $CuSe_4$ tetrahedra and flat $SbSe_4$ tetrahedra, which enhance phonon scattering [3]. Permingeatite is of particular interest because it can result in low thermal conductivity through anharmonic vibrations [4]. In addition, its large effective mass ($\approx 1.1\ m_o$) and narrow band gap (0.29-0.40 eV) are advantageous for thermoelectric applications [5].

Thermoelectric performance is evaluated based on a power factor ($PF = \alpha^2\sigma$) and dimensionless figure-of-merit ($ZT = \alpha^2\sigma\kappa^{-1}T$), which is affected by the Seebeck coefficient (α), electrical conductivity (σ), and thermal conductivity (κ) of a material at the application temperature (T, in units of Kelvin). To improve the thermoelectric performance of permingeatite, a number of studies have focused on substitution (doping) at the Cu site. For example, Kumar et al. [6,7] reported ZT values of 0.35 at 475 K for $Cu_{2.5}Zn_{0.5}SbSe_4$ and 0.65 at 650 K for $Cu_{2.99}Ni_{0.01}SbSe_4$. Doping of various elements at Sb sites has been extensively reported on efforts to reduce thermal conductivity by phonon scattering. Zhao et al. [8] reported a ZT of 0.54 at 605 K for $Cu_3Sb_{0.985}Ga_{0.015}Se_4$; Chang et al. [9] obtained a ZT of 0.54 at 640 K for $Cu_{2.95}Sb_{0.96}Ge_{0.04}Se_4$; Zhang et al. [10] achieved a ZT of 0.50 at 648 K for $Cu_3Sb_{0.997}In_{0.003}Se_4$; Li et al. [11] reported a ZT of 0.58 at 600 K for $Cu_3Sb_{0.97}Al_{0.03}Se_4$. In addition, Kumar et

- 안희재: 학사과정, 김일호: 교수
*Corresponding Author: Il-Ho Kim
[Tel: +82-43-841-5387, E-mail: ihkim@ut.ac.kr]

al. [12] investigated double doping at Sb and Se sites and reported a ZT of 0.76 at 650 K for $Cu_3Sb_{0.98}Bi_{0.02}Se_{3.99}Te_{0.01}$. Liu et al. [13] obtained a high ZT of 1.26 at 673 K for $Cu_3Sb_{0.88}Sn_{0.1}Bi_{0.02}Se_4$, where Sn and Bi were double doped at the Sb site using a multistep solution-based synthesis.

In our previous study [14], famatinite (Cu_3SbS_4; space group $I\bar{4}2\,m$) with a crystal structure similar to that of permingeatite was successfully and easily synthesized via mechanical alloying (MA) as a one-step solid-state method without subsequent heat treatment. In this study, $Cu_3Sb_{1-x-y}Sn_xBi_ySe_4$ with partial double doping at the Sb site was prepared via MA and hot pressing (HP), and the effects of double doping Sn and Bi on thermoelectric performance were investigated.

2. EXPERIMENTAL PROCEDURE

Sn/Bi double-doped permingeatites $Cu_3Sb_{1-x-y}Sn_xBi_ySe_4$ (x = 0.02, 0.04, and 0.06; y = 0.02 and 0.04) were synthesized via MA. The compositions of the specimens were designed to be x + y = 0.06 or 0.08. Cu (< 45 μm, purity 99.9%), Sb (< 150 μm, purity 99.999%), Sn (< 35 μm, purity 99.999%), Bi (< 180 μm, purity 99.999%), and Se (< 10 μm, purity 99.9%) powders were used as the starting materials for MA. A planetary ball milling system (Pulverisette5, Fritsch) was employed with hardened steel jars and balls, and MA was conducted at 350 rpm for 12 h in an Ar atmosphere. Then, the synthesized powder was consolidated using HP at 573 K for 2 h under 70 MPa in vacuum.

X-ray diffraction (XRD; D8-Advance, Bruker) was performed using Cu–Kα radiation to analyze the phases of the specimens. The lattice constants were estimated using Rietveld refinement (TOPAS, Bruker). Scanning electron microscopy (SEM; Quanta400, FEI) was performed to observe the microstructures of the HP specimens. The chemical composition was analyzed using energy-dispersive spectroscopy (EDS; Quantax200, Oxford Instruments). The van der Pauw (7065, Keithley) method was used and a single-valley model was assumed to measure the charge transport parameters under the conditions of 1 T and 100 mA_{DC}. A four-probe system (ZEM-3, Advance Riko) was used to measure the Seebeck coefficient and electrical conductivity. Laser flash equipment (TC-9000H, Advance Riko) was used to measure the thermal diffusivity, and the thermal conductivity was calculated using the density and specific heat of the specimens. Finally, the PF and ZT values were evaluated.

3. RESULTS AND DISCUSSION

Fig. 1 shows the results of the phase analysis of $Cu_3Sb_{1-x-y}Sn_xBi_ySe_4$ synthesized via MA–HP. Phase changes caused by Sn and Bi contents were not observed, and a single-phase tetragonal permingeatite (ICDD PDF#085–0003) was achieved. The lattice constant of $Cu_3Sb_{1-x-y}Sn_xBi_ySe_4$, as shown in Table 1, decreased from 0.56518 to 0.56515 nm for

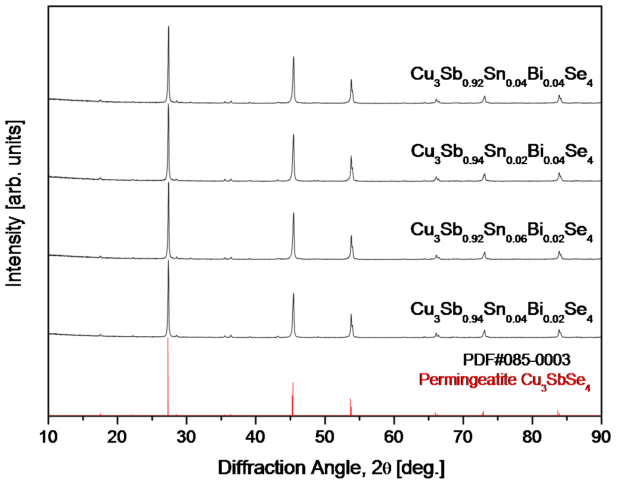

Fig. 1. XRD patterns of $Cu_3Sb_{1-x-y}Sn_xBi_ySe_4$ permingeatite synthesized via mechanical alloying and hot pressing.

Table 1. Chemical compositions and physical properties of $Cu_3Sb_{1-x-y}Sn_xBi_ySe_4$.

Composition		Relative density	Lattice constant [nm]		Lorenz number
Nominal	Actual	[%]	a	c	[10^{-8} V^2K^{-2}]
$Cu_3Sb_{0.94}Sn_{0.04}Bi_{0.02}Se_4$	$Cu_{3.06}Sb_{0.78}Sn_{0.04}Bi_{0.06}Se_{4.03}$	97.7	0.56518	1.12525	1.93
$Cu_3Sb_{0.92}Sn_{0.06}Bi_{0.02}Se_4$	$Cu_{3.37}Sb_{0.81}Sn_{0.06}Bi_{0.04}Se_{4.03}$	97.8	0.56510	1.12529	1.96
$Cu_3Sb_{0.94}Sn_{0.02}Bi_{0.04}Se_4$	$Cu_{3.07}Sb_{0.82}Sn_{0.02}Bi_{0.08}Se_{3.99}$	98.2	0.56516	1.12509	1.79
$Cu_3Sb_{0.92}Sn_{0.04}Bi_{0.04}Se_4$	$Cu_{2.96}Sb_{0.86}Sn_{0.06}Bi_{0.07}Se_{4.02}$	98.1	0.56515	1.12515	1.87

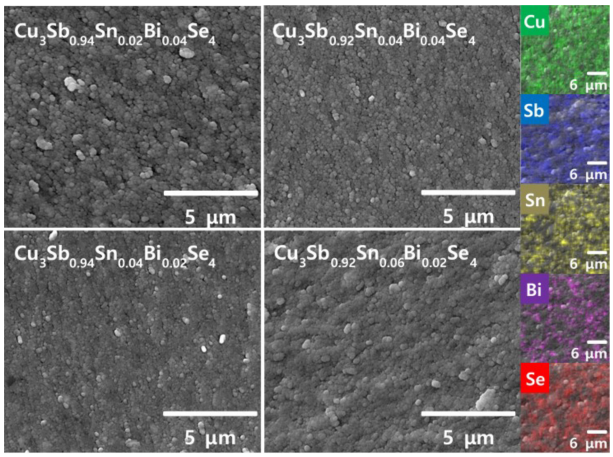

Fig. 2. SEM images of fractured surfaces for $Cu_3Sb_{1-x-y}Sn_xBi_ySe_4$ and EDS elemental maps of $Cu_3Sb_{0.92}Sn_{0.06}Bi_{0.02}Se_4$.

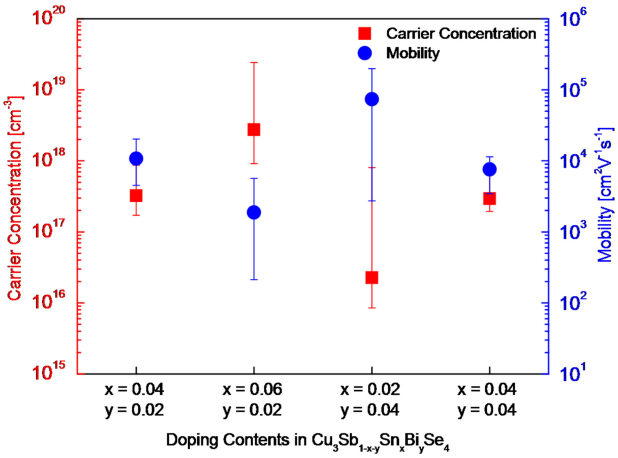

Fig. 3. Charge transport properties of $Cu_3Sb_{1-x-y}Sn_xBi_ySe_4$.

the a-axis and from 1.12525 to 1.12515 nm for the c-axis as the Bi content increased. However, as the Sn content increased, that of the a-axis decreased to 0.56510 nm, but that of the c-axis increased to 1.12529 nm. Because the lattice constants of undoped Cu_3SbSe_4 are a = 0.564 nm and c = 1.128 nm [13, 15], when Sn and Bi were double doped in this study, the a-axis increased, and the c-axis decreased. Prasad et al. [16] reported that as the Sn content of $Cu_3Sb_{1-x}Sn_xSe_4$ (x = 0.00-0.04) increased, the degree of disorder at the cation site increased, and the lattice volume decreased because of a decrease in the anti-site defect Sn_{Sb} or an increase in Sb_{Sn}. In contrast, Yang et al. [17] reported that the lattice of $Cu_3Sb_{1-x}Sn_xSe_4$ (x = 0-0.05) expanded with Sn content, owing to the larger ionic radius of Sn^{4+} compared with that of Sb^{5+}. Li et al. [18] suggested the occurrence of lattice distortion and point defects (V_{Cu} or V_{Sb}); hence, the lattice constant increased when Bi was doped at the Sb site because the radius of Bi^{5+} was larger than that of Sb^{5+}. Liu et al. [13] discovered that lattice expansion occurred because of the simultaneous replacement of the larger cations Sn^{4+} (69 pm) and Bi^{5+} (76 pm) compared with that of Sb^{5+} (60 pm).

Fig. 2 presents the fractured surfaces of sintered $Cu_3Sb_{1-x-y}Sn_xBi_ySe_4$. It was observed that the Sn and Bi contents did not affect the microstructure. In addition, no unreacted residual elements or secondary phases were observed. The right column in the SEM images shows the EDS elemental maps of $Cu_3Sb_{0.92}Sn_{0.06}Bi_{0.02}Se_4$, which indicate that each element was homogeneously distributed. The relative density of the Sn/Bi double-doped permingeatite was 97.7%–98.2% (Table 1); the actual and nominal compositions did not differ significantly, and they were within the measurement error range. Therefore, a single permingeatite phase double-doped with Sn and Bi was successfully synthesized via MA and HP.

The charge transport characteristics of $Cu_3Sb_{1-x-y}Sn_xBi_ySe_4$ are shown in Fig. 3. The Hall coefficient values were positive, confirming that the majority charge carrier was holes in the p-type semiconductor. When the Bi content (y) was constant, the carrier concentration increased with the Sn content (x), i.e., from 3.24×10^{17} to 2.75×10^{18} cm^{-3} when y = 0.02, and from 2.28×10^{16} to 2.93×10^{17} cm^{-3} when y = 0.04. This was due to the additional holes generated by doping Sn^{4+} at the Sb^{5+} site. When the Sn content was constant, the change in the carrier concentration was insignificant, based on the Bi content. This was attributed to the valences of Bi^{5+} and Sb^{5+}. Wei et al. [5] reported that Sn doping increased the carrier concentration of $Cu_{2.95}Sb_{1-x}Sn_xSe_4$ (x = 0.00-0.04) from 5.02×10^{19} to 2.08×10^{20} cm^{-3}. Li et al. [18] achieved an increased carrier concentration in $Cu_3Sb_{1-y}Bi_ySe_4$ (y = 0.00-0.03), i.e., from 3.38×10^{18} to 7.21×10^{18} cm^{-3}; however, it decreased to 2.89×10^{18} cm^{-3} when y = 0.03 owing to the presence of impurity phases.

In this study, when the Bi content was constant, the mobility decreased significantly as the Sn content increased, i.e., from 1.07×10^4 to 1.88×10^3 $cm^2V^{-1}s^{-1}$ when y = 0.02 and from 7.39×10^4 to 7.59×10^3 $cm^2V^{-1}s^{-1}$ when y = 0.04. However, when the Sn content was constant, the mobility

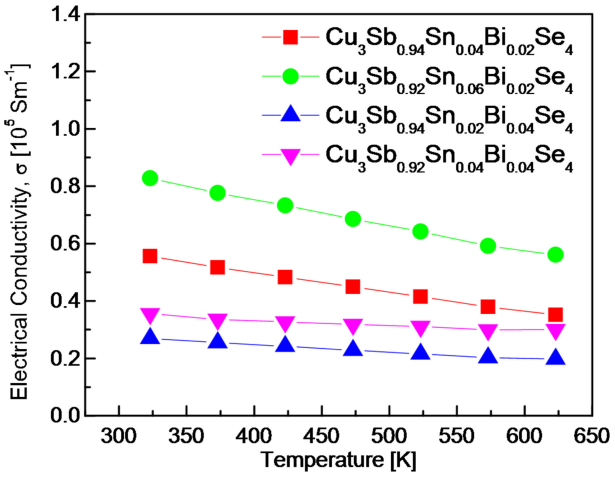

Fig. 4. Temperature dependence of electrical conductivity for $Cu_3Sb_{1-x-y}Sn_xBi_ySe_4$.

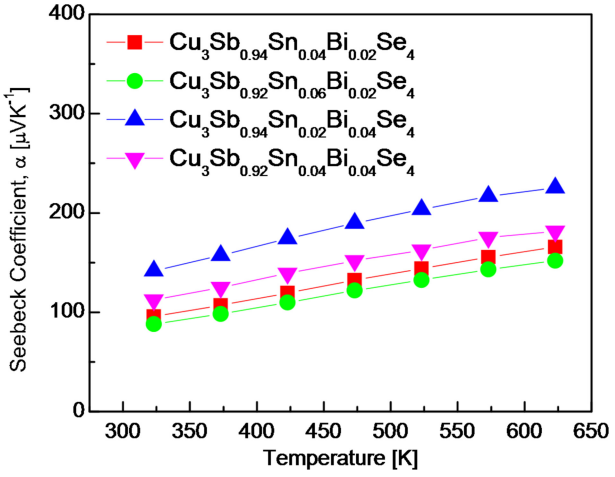

Fig. 5. Temperature dependence of Seebeck coefficient for $Cu_3Sb_{1-x-y}Sn_xBi_ySe_4$.

slightly decreased from 1.07×10^4 to 7.59×10^3 $cm^2V^{-1}s^{-1}$ depending on the Bi content. Wei et al. [5] reported that as the Sn content increased in $Cu_3Sb_{1-x}Sn_xSe_4$ (x = 0.01-0.04), the mobility decreased from 49 to 26 $cm^2V^{-1}s^{-1}$. Li et al. [18] reported that as the Bi content increased in $Cu_3Sb_{1-y}Bi_ySe_4$ (y = 0.01-0.03), the mobility decreased from 1.65×10^2 to 1.06×10^2 $cm^2V^{-1}s^{-1}$.

Fig. 4 shows the electrical conductivity of $Cu_3Sb_{1-x-y}Sn_xBi_ySe_4$. The electrical conductivity of a degenerate semiconductor is defined as $\sigma = en\mu$ (where e, n and μ are the electronic charge, the carrier concentration and the mobility, respectively) [19]. Therefore, electrical conductivity is affected by the temperature dependence of the carrier concentration and mobility. When the Bi content (y) was constant, the electrical conductivity increased with the Sn content (x), because of the increase in carrier concentration. In the temperature range of 323-623 K, the electrical conductivity increased from $(5.56\text{-}3.51) \times 10^4$ to $(8.28\text{-}5.61) \times 10^4$ Sm^{-1} for x = 0.04-0.06 when y = 0.02, whereas it increased from $(2.69\text{-}1.97) \times 10^4$ to $(3.56\text{-}3.00) \times 10^4$ Sm^{-1} for x = 0.02-0.04 when y = 0.04. However, when the Sn content was constant, the electrical conductivity decreased slightly as the Bi content increased, due to changes in the carrier concentration and mobility, as shown in Fig. 3. Consequently, $Cu_3Sb_{0.92}Sn_{0.06}Bi_{0.02}Se_4$ exhibited the highest electrical conductivity, whereas $Cu_3Sb_{0.94}Sn_{0.02}Bi_{0.04}Se_4$ exhibited the lowest electrical conductivity.

Lee et al. [20] reported that the minimum electrical conductivity of Cu_3SbSe_4 was $(4.23\text{-}4.88) \times 10^3$ Sm^{-1} at 323-623 K, which indicated nondegenerate semiconductor behavior. Compared with the undoped permingeatite, the electrical conductivity of permingeatite double-doped with Sn/Bi improved significantly in this study. Wei et al. [5] reported that electrical conductivity increased with Sn content in $Cu_3Sb_{1-x}Sn_xSe_4$ (x = 0.01-0.04), where the highest electrical conductivity was 4.76×10^3 Sm^{-1} at 673 K for $Cu_3Sb_{0.96}Sn_{0.04}Se_4$. Li et al. [18] obtained the highest electrical conductivity of 1.11×10^4 Sm^{-1} at 600 K for $Cu_3Sb_{0.98}Bi_{0.02}Se_4$, among $Cu_3Sb_{1-y}Bi_ySe_4$ (y = 0.01-0.03). Liu et al. [13] investigated double-doped $Cu_3Sb_{1-x-y}Sn_xBi_ySe_4$ (x = 0.02-0.10 and y = 0.02) and obtained the highest electrical conductivity of 7.85×10^4 Sm^{-1} at 673 K for $Cu_3Sb_{0.88}Sn_{0.10}Bi_{0.02}Se_4$.

Fig. 5 shows the Seebeck coefficients of $Cu_3Sb_{1-x-y}Sn_xBi_ySe_4$. The permingeatite double-doped with Sn/Bi was a p-type semiconductor, which was reconfirmed from the positive Seebeck coefficient. The Seebeck coefficient is defined as $a = (8/3)(\pi/3n)^{2/3}(\pi k_B/h)^2 m^* Te^{-1}$ (where k_B, h and m^* are the Boltzmann constant, the Planck constant and the effective carrier mass, respectively) [21]. Because the Seebeck coefficient is inversely proportional to carrier concentration, it exhibits an opposite trend to the electrical conductivity. At a constant temperature, when the Bi content was constant, the Seebeck coefficient decreased with increasing Sn content, whereas when the Sn content was constant, the Seebeck coefficient increased with Bi content. Consequently,

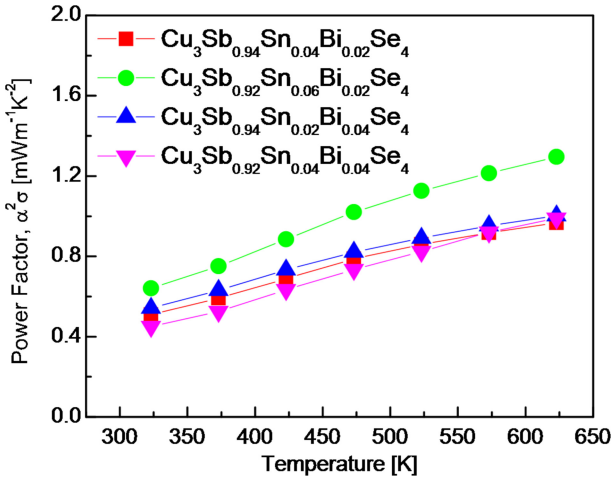

Fig. 6. Temperature dependence of power factor for $Cu_3Sb_{1-x-y}Sn_xBi_ySe_4$.

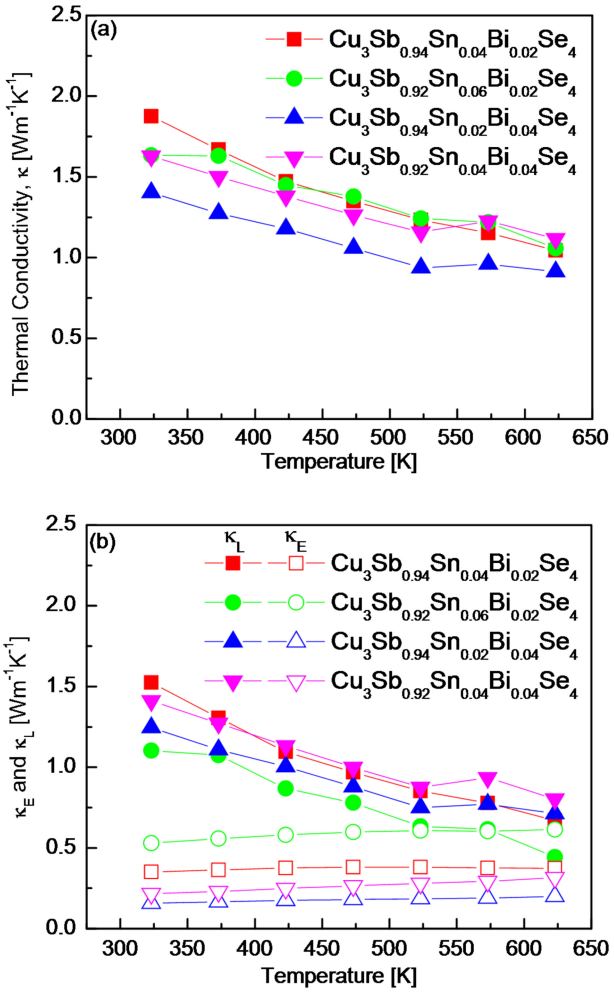

Fig. 7. Temperature dependence of thermal conductivities of $Cu_3Sb_{1-x-y}Sn_xBi_ySe_4$: (a) Total thermal conductivity and (b) electronic and lattice thermal conductivities.

$Cu_3Sb_{0.94}Sn_{0.02}Bi_{0.04}Se_4$ exhibited a maximum Seebeck coefficient of 141-225 μVK^{-1} at 323-623 K. Lee et al. [20] reported a Seebeck coefficient of 312-330 μVK^{-1} at 323-623 K for undoped Cu_3SbSe_4. Wei et al. [5] obtained a lower Seebeck coefficient by doping Sn into $Cu_{2.95}Sb_{1-x}Sn_xSe_4$ (x = 0.01-0.04); they obtained a maximum Seebeck coefficient of 163-249 μVK^{-1} at 300-673 K for $Cu_3Sb_{0.99}Sn_{0.01}Se_4$. Li et al. [18] discovered that an intrinsic transition occurred at temperatures above 400 K for $Cu_3Sb_{1-x}Bi_xSe_4$ (x = 0.01-0.03), which resulted in a maximum Seebeck coefficient of 417 μVK^{-1} at 400 K for $Cu_3Sb_{0.98}Bi_{0.02}Se_4$. Liu et al. [13] reported that the double doping of Sn and Bi effectively increased the Seebeck coefficient of $Cu_3Sb_{1-x-y}Sn_xBi_ySe_4$ (x = 0.02-0.10 and y = 0.02), and that $Cu_3Sb_{0.96}Sn_{0.02}Bi_{0.02}Se_4$ achieved a maximum Seebeck coefficient of 149-279 μVK^{-1} at 323-673 K.

Fig. 6 shows the PF of $Cu_3Sb_{1-x-y}Sn_xBi_ySe_4$. The PF depends on the electrical conductivity and Seebeck coefficient, and these two parameters are affected oppositely by the carrier concentration [22]. The PF increased with temperature because the effect of increasing the Seebeck coefficient was greater than that of decreasing electrical conductivity caused by an increase in temperature. At a constant temperature, however, the increase in electrical conductivity by Sn/Bi double doping was more effective at increasing the PF than the decrease in the Seebeck coefficient. Consequently, $Cu_3Sb_{0.92}Sn_{0.06}Bi_{0.02}Se_4$ achieved the highest PF of 0.64-1.29 mWm^{-1}K^{-2} at 323-623 K. Compared with the PF of undoped Cu_3SbSe_4 (0.38-0.50 mWm^{-1}K^{-2} at 323-623 K) [20], Cu_3SbSe_4 double-doped with Sn/Bi significantly increased the PF of permingeatite. Wei et al. [5] obtained a PF of 0.65-1.38 mWm^{-1}K^{-2} at 300-673 K for $Cu_3Sb_{0.97}Sn_{0.03}Se_4$. Li et al. [18] reported that the PF decreased with temperature from 1.8 mWm^{-1}K^{-2} at 323 K to 1.1 mWm^{-1}K^{-2} at 600 K for $Cu_3Sb_{0.98}Bi_{0.02}Se_4$. In fact, Liu et al. [13] further increased the Seebeck coefficient by performing Sn/Bi double doping (as compared with only Sn doping) and achieved the highest PF of 1.81 mWm^{-1}K^{-2} at 654 K for $Cu_3Sb_{0.88}Sn_{0.1}Bi_{0.02}Se_4$.

The thermal conductivities of $Cu_3Sb_{1-x-y}Sn_xBi_ySe_4$ are shown in Fig. 7. After determining the electronic thermal

conductivity (κ_E) using the Wiedemann–Franz law ($\kappa_E = L\sigma T$), the lattice thermal conductivity (κ_L) was calculated from the measured thermal conductivity (κ) using the relation $\kappa = \kappa_E + \kappa_L$ [23,24], where the temperature-dependent Lorenz number (L) was estimated using the equation $L = 1.5 + \exp(-|\alpha|/116)$ [25, 26]. In this study, a specific heat of 0.32 $Jg^{-1}K^{-1}$ was used to evaluate the thermal conductivity [27], and Fig. 7(a) shows the thermal conductivity of $Cu_3Sb_{1-x-y}Sn_xBi_ySe_4$. The thermal conductivity decreased with temperature, and bipolar conduction did not occur within the measurement temperature range. At a constant temperature, the thermal conductivity decreased at higher Bi and lower Sn contents. However, a lower thermal conductivity was obtained at 523 K as the Bi content increased when the Sn content was constant at $x = 0.04$. Additionally, higher thermal conductivity was observed at temperatures above 523 K. This crossover in the thermal conductivity was similarly reported in Bi-doped permingeatite by Li et al. [18]. In this study, the lowest thermal conductivity of 1.40-0.91 $Wm^{-1}K^{-1}$ was obtained at 323-623 K in $Cu_3Sb_{0.94}Sn_{0.02}Bi_{0.04}Se_4$. Wei et al. [5] reported a minimum thermal conductivity of 3.19-1.21 $Wm^{-1}K^{-1}$ at 275-700 K for $Cu_{2.95}Sb_{0.99}Sn_{0.01}Se_4$. Li et al. [18] obtained a minimum thermal conductivity of 1.97-0.98 $Wm^{-1}K^{-1}$ at 323-573 K for $Cu_3Sb_{0.98}Bi_{0.02}Se_4$. Liu et al. [13] reported the lowest thermal conductivity of 1.20-0.94 $Wm^{-1}K^{-1}$ at 323-673 K in $Cu_3Sb_{0.96}Sn_{0.02}Bi_{0.02}Se_4$.

Fig. 7(b) shows the separate contributions to thermal conductivity. κ_E was attributed to the charge carriers, and κ_L was due to phonons. κ_E did not indicate a significant temperature dependence; however, it was directly affected by the carrier concentration, i.e., the Sn/Bi doping concentration. κ_E decreased because of the reduced carrier concentration as the Bi content increased and the Sn content decreased. Hence, a minimum κ_E of 0.15-0.19 $Wm^{-1}K^{-1}$ was achieved at 323-623 K in $Cu_3Sb_{0.94}Sn_{0.02}Bi_{0.04}Se_4$.

The κ_E values achieved in other studies were as follows: 0.18-0.17 $Wm^{-1}K^{-1}$ at 275-700 K for $Cu_3Sb_{0.9}Sn_{0.1}Se_4$ [5], 0.05-0.11 $Wm^{-1}K^{-1}$ at 323-575 K for $Cu_3Sb_{0.7}Bi_{0.3}Se_4$ [18], and 0.15-0.22 $Wm^{-1}K^{-1}$ at 323-673 K for $Cu_3Sb_{0.96}Sn_{0.02}Bi_{0.02}Se_4$ [13]. In this study, κ_L decreased as the temperature increased. When the Bi content was constant at 0.02, κ_L was lower as the Sn content increased; consequently, the lowest κ_L of 1.10-0.44 $Wm^{-1}K^{-1}$ was obtained at 323-623 K in $Cu_3Sb_{0.92}Sn_{0.06}Bi_{0.02}Se_4$.

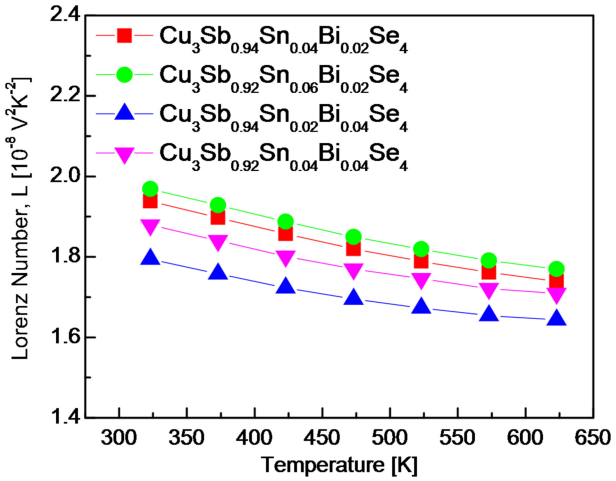

Fig. 8. Temperature dependence of Lorenz number for $Cu_3Sb_{1-x-y}Sn_xBi_ySe_4$.

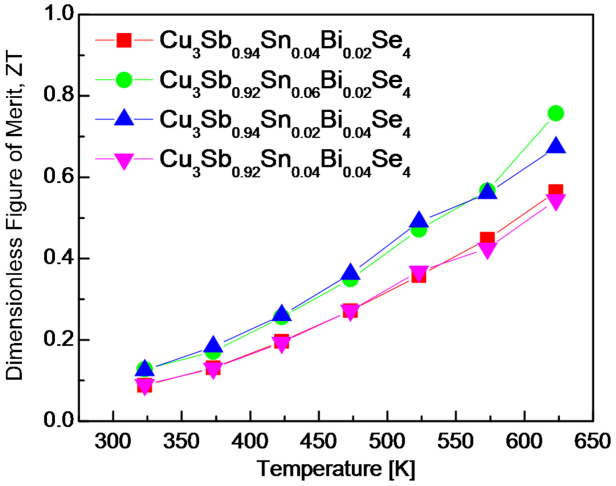

Fig. 9. Dimensionless figure of merit for $Cu_3Sb_{1-x-y}Sn_xBi_ySe_4$.

However, when the Bi content increased to 0.04, κ_L increased as the Sn content increased. Therefore, when the Bi doping level was low, the addition of Sn effectively reduced κ_L, whereas when the Sn doping level was low, the addition of Bi effectively reduced κ_E. Wei et al. [5] reported that the κ_L of all samples of $Cu_{2.95}Sb_{1-x}Sn_xSe_4$ ($x = 0.01$-0.04) was 2.81-1.01 $Wm^{-1}K^{-1}$ at 275-700 K. Li et al. [18] obtained a minimum κ_L of 1.87-0.79 $Wm^{-1}K^{-1}$ at 323-573 K for $Cu_3Sb_{0.97}Bi_{0.03}Se_4$. Liu et al. [13] achieved the lowest κ_L of 0.89-0.27 $Wm^{-1}K^{-1}$ at 323-673 K for $Cu_3Sb_{0.88}Sn_{0.1}Bi_{0.02}Se_4$.

Fig. 8 shows the L of $Cu_3Sb_{1-x-y}Sn_xBi_ySe_4$. Theoretically, the range of L is $(1.45\text{-}2.44) \times 10^{-8}$ V^2K^{-2}; higher numbers indicate degenerate semiconductor or metallic behavior,

whereas smaller numbers indicate nondegenerate semiconductor behavior [21, 28]. A maximum L of (1.96-1.76) × 10^{-8} V^2K^{-2} was obtained at 323-623 K in $Cu_3Sb_{0.92}Sn_{0.06}Bi_{0.02}Se_4$, whereas a minimum L of (1.79-1.64) × 10^{-8} V^2K^{-2} was achieved at 323-623 K in $Cu_3Sb_{0.94}Sn_{0.02}Bi_{0.04}Se_4$. Sn doping increased L (shifted to the degenerate state); conversely, Bi doping decreased L (shifted to the nondegenerate state). Lee et al. [20] reported a L of (1.54-1.56) × 10^{-8} V^2K^{-2} at 323-623 K for undoped Cu_3SbSe_4.

Fig. 9 presents the ZT of $Cu_3Sb_{1-x-y}Sn_xBi_ySe_4$. The highest ZT of 0.75 was obtained at 623 K in $Cu_3Sb_{0.92}Sn_{0.06}Bi_{0.02}Se_4$, the result of its high PF and low thermal conductivity. Although the thermal conductivity was the lowest when x = 0.02 and y = 0.04, the maximum ZT value was attributed to the highest PF, when x = 0.06 and y = 0.02. Lee et al. [20] reported a ZT of 0.39 at 623 K for undoped Cu_3SbSe_4, which was synthesized via the same process as ours; the reported ZT value was approximately two times higher than that achieved via Sn/Bi double doping. Wei et al. [5] reported a ZT of 0.70 at 673 K for $Cu_3Sb_{0.98}Sn_{0.02}Se_4$ synthesized via MA and spark plasma sintering (SPS). Li et al. [18] obtained a ZT of 0.70 at 600 K for $Cu_3Sb_{0.98}Bi_{0.02}Se_4$ synthesized via melting–SPS. Liu et al. [13] achieved an extremely high ZT of 1.26 at 673 K for $Cu_3Sb_{0.88}Sn_{0.10}Bi_{0.02}Se_4$ prepared via a multistep solution-based synthesis followed by HP; the thermal conductivity was approximately 1 $Wm^{-1}K^{-1}$, which was similar to our result, but the PF was 1.81 $mWm^{-1}K^{-2}$ (an anomalously high value for permingeatite), which was 1.4 times higher than ours (1.29 $mWm^{-1}K^{-2}$). These values were obtained because the carrier concentration was ≈10^{20} cm^{-3}, which was two orders higher compared with that of our specimen. In addition to the doping level, the measured temperature of the thermoelectric properties was higher than 623 K, which contributed to the high ZT value because it was proportional to the measured temperature below the temperature at which the intrinsic transition and bipolar conduction occurred.

4. CONCLUSIONS

Permingeatite $Cu_3Sb_{1-x-y}Sn_xBi_ySe_4$ (x = 0.02–0.06, y = 0.02–0.04) double-doped with Sn and Bi at the Sb site was synthesized via MA–HP. XRD analysis revealed that both the synthetic powders and sintered specimens investigated in this study were composed of a tetragonal permingeatite phase without secondary phases. All elements in the sintered samples were distributed uniformly, with a relative density of 97.7%–98.2%. After Sn and Bi were substituted at the Sb site, the lattice constant changed to 0.56510-0.56518 nm for the a-axis and 1.12509-1.12529 nm for the c-axis. The Hall and Seebeck coefficients were positive, thereby confirming that the Sn/Bi double-doped permingeatite is a p-type semiconductor. Sn doping resulted in charge compensation due to additional electrons; hence, the carrier concentration increased from 2.27 × 10^{16} to 2.74 × 10^{18} cm^{-3}, whereas the mobility decreased from 7.39 × 10^4 to 1.88 × 10^3 cm^2Vs^{-1}. However, Bi doping did not significantly affect the charge transport properties. As the Sn content increased and the Bi content decreased, the electrical conductivity increased, where the highest electrical conductivity of (8.28-5.61) × 10^4 Sm^{-1} was exhibited at 323-623 K in $Cu_3Sb_{0.92}Sn_{0.06}Bi_{0.02}Se_4$. In contrast, as the Sn content decreased and the Bi content increased, the Seebeck coefficient increased, resulting in the highest Seebeck coefficient of 141-225 μVK^{-1} at 323-623 K in $Cu_3Sb_{0.94}Sn_{0.02}Bi_{0.04}Se_4$. Consequently, $Cu_3Sb_{0.92}Sn_{0.06}Bi_{0.02}Se_4$ exhibited a maximum PF of (0.64-1.29) $mWm^{-1}K^{-2}$ at 323-623 K. Sn doping decreased the lattice thermal conductivity, whereas Bi doping reduced the electronic thermal conductivity but did not effectively reduce the lattice thermal conductivity. The lowest thermal conductivity of 1.40-0.91 $Wm^{-1}K^{-1}$ was obtained at 323-623 K in $Cu_3Sb_{0.94}Sn_{0.02}Bi_{0.04}Se_4$. Consequently, a maximum ZT of 0.75 was achieved at 623 K by $Cu_3Sb_{0.92}Sn_{0.06}Bi_{0.02}Se_4$.

Acknowledgment

This study was supported by the Basic Science Research Capacity Enhancement Project (National Research Facilities and Equipment Center) through the Korea Basic Science Institute funded by the Ministry of Education (Grant No. 2019R1A6C1010047).

REFERENCES

1. M. Irfan, Z. Abbas, S. Khan, M. Sohail, M. Rani, S. Azam, and I. V. Kityk, *J. Alloys Compd.* **750**, 804 (2018).

2. A. Kumar, P. Dhama, and P. Banerji, *AIP Conf. Proc.* **1832**, 110050 (2017).
3. D. Li, R. Li, X. Y. Qin, J. Zhang, C. J. Song, L. Wang, and H. X. Xim, *CrystEngComm*, **15**, 7166 (2013).
4. Y. Zhang, E. Skoug, J. Cain, V. Ozolins, D. Morelli, and C. Wolverton, *Phys. Rev. B* **85**, 054306 (2012).
5. T. R. Wei, H. Wang, Z. M. Gibbs, C. F. Wu, G. J. Snyder, and J. F. Li, *J. Mater. Chem*. *A* **2**, 13527 (2014).
6. A. Kumar, P. Dhama, D. S. Saini, and P. Banerji, *RSC Adv.* **6**, 5528 (2016).
7. A. Kumar, P. Dhama, A. Das, K. J. Sarkar, and P. Banerji, *AIP Conf. Proc.* **1953**, 050030 (2018).
8. D. Zhao, D. Wu, and L. Bo, *Energies* **10**, 1524 (2017).
9. C. H. Chang, C. L. Chen, W. T. Chiu, and Y. Y. Chen, *Mater. Lett*. **186**, 227 (2017).
10. D. Zhang, J. Yang, Q. Jiang, L. Fu, Y. Xiao, Y. Luo, and Z. Zhou, *Mater. Des*. **98**, 150 (2016).
11. Y. Li, X. Qin, D. Li, X. Li, Y. Liu, J. Zhang, C. Song, and H. Xin, *RSC Adv.* **5**, 31399 (2015).
12. A. Kumar, P. Dhama, and P. Banerji, *AIP Conf. Proc*. **1942**, 140055 (2018).
13. Y. Liu, G. Garcia, S. Ortega, D. Cadavid, P. Palacios, J. Lu, M. Ibanez, L. Xi, J. D. Roo, A. M. Lopez, S. M. Sanchez, I. Cabezas, M. D. L. Mata, Z. Luo, C. Dun, O. Dobrozhan, D. L. Carroll, W. Zhang, J. Martins, M. V. Kovalenko, J. Arbiol, G. Noriega, J. Song, P. Wahnon, and A. Cabot, *J. Mater. Chem. A* **5**, 2592 (2017).
14. G. E. Lee, J. H. Pi, and I. H. Kim, *J. Electron. Mater*. **49**, 2781 (2020).
15. Y. Dou, Q. Zhu, Y. Du, J. Xu, and D. Li, *Electron. Mater. Lett*. **16**, 99 (2020).
16. K. S. Prasad and A. Rao, *J. Mater Sci: Mater. Electron*. **30**, 16596 (2019).
17. C. Yang, F. Huang, L. Wu, and K. Xu, *J. Phys. D: Appl. Phys.* **44**, 295404 (2011).
18. X. Y. Li, D. Li, H. X. Xin, J. Zhang, C. J. Song, and X. Y. Qin, *J. Alloys Compd.* **561**, 105 (2013).
19. X. Shi, H. Chen, F. Hao, R. Liu, T. Wang, P. Qiu, U. Burkhardt, Y. Grin, and L. Chen, *Nat. Mater*. **17**, 421 (2018).
20. G. E. Lee and I. H. Kim, *Materials* **14**, 1116 (2021).
21. H. S. Kim, Z. M. Gibbs, Y. Tang, H. Wang, and G. J. Snyder, *APL Mater*. **3**, 041506 (2015).
22. G. J. Snyder and E. S. Toberer, *Nat. Mater*. **7**, 105 (2008).
23. T. Caillat, A. Borshchevsky, and J. P. Fleurial, *J. Appl. Phys*. **80**, 4442 (1996).
24. S. Y. Kim, J. H. Pi, G. E. Lee, and I. H. Kim, *Korean J. Met. Mater.* **58**, 340 (2020).
25. B. Madaval and S. J. Hong, *J. Electron. Mater*. **45**, 6059 (2016).
26. S. G. Kwak, J. H. Pi, G. E. Lee, and I. H. Kim, *Korean J. Met. Mater.* **58**, 272 (2020).
27. O. Madalung, *Semiconductors: Basic Data*, 2nd ed., p.267, Springer, Berlin (1996).
28. E. J. Skoung, J. D. Cain, D. T. Morelli, M. Kirkham, P. Majsztrik, and E. Lara-Curzio, *J. Appl. Phys*. **110**, 023501 (2011).